Photocathodes

DOI: 10.1002/anie.201310461

Aqueous-Solution Route to Zinc Telluride Films for Application to CO_2 Reduction**

Ji-Wook Jang, Seungho Cho, Ganesan Magesh, Youn Jeong Jang, Jae Young Kim, Won Yong Kim, Jeong Kon Seo, Sungjee Kim, Kun-Hong Lee, and Jae Sung Lee**

Abstract: *As a photocathode for CO_2 reduction, zinc-blende zinc telluride (ZnTe) was directly formed on a Zn/ZnO nanowire substrate by a simple dissolution–recrystallization mechanism without any surfactant. With the most negative conduction-band edge among p-type semiconductors, this new photocatalyst showed efficient and stable CO formation in photoelectrochemical CO_2 reduction at −0.2−−0.7 V versus RHE without a sacrificial reagent.*

Zinc telluride, with a direct band gap of 2.26 eV[1] and a Bohr exciton radius of 6.2 nm,[2] is a very attractive II–IV semiconductor for optoelectronic devices, such as blue–green light-emitting diodes,[3] electrooptical detectors,[4] and solar cells.[5] ZnTe has been synthesized by various methods, most of which are based on colloidal synthesis.[1–3,7,9–14] However, it is still a challenge to obtain stable ZnTe in aqueous solution without the help of a surfactant. In this study, we fabricated ZnO/ZnTe heterostructures by a dissolution–recrystallization mechanism in an aqueous solution. Thus, ZnO nanowires on a zinc metal substrate were transformed into ZnTe through a reaction with tellurite and hydrazine in an aqueous solution. This process is the simplest way to synthesize ZnTe in an aqueous solution without using a surfactant. Since ZnTe is directly formed on the Zn/ZnO electrode, it could be readily applied as an electrode for an optoelectronic device.

The conversion of CO_2 into fuels by the use of a renewable energy is considered an ideal and practical solution to next-generation energy problems, as these fuels can be readily stored and utilized in the existing infrastructures with minimal changes. The best available option for the conversion is the photoelectrochemical (PEC) reduction of CO_2 in a similar manner to that operating in natural photosynthesis.[15–18] The most important challenge in the successful design of such a process is the development of photoelectrode materials that absorb stable solar photons and convert them efficiently into chemical energy in combination with molecular and/or inorganic cocatalysts.[19–21]

A salient feature of ZnTe is the most negative conduction-band-edge position (−1.63 V versus the reversible hydrogen electrode (RHE)) of all p-type semiconductors known so far, which leads to a large driving force for interfacial electron transfer from the semiconductor to acceptors.[6,7] Naturally, we consider that ZnTe is a very promising photocathode material, especially for PEC solar-fuel production, in which sluggish kinetics of CO_2 reduction lead to high overpotentials.[8] Surprisingly, however, there has been no report, to the best of our knowledge, of the use of a ZnTe photocathode for CO_2 reduction. In the present study, we investigated a ZnTe electrode for the first time as a photocathode for PEC CO_2 reduction.

Our unique fabrication of a ZnTe film started with the growth of ZnO nanowires on a zinc metal substrate in a zinc acetate solution according to a procedure reported elsewhere.[22] Zinc-blende ZnTe was directly formed on the Zn/ZnO nanowire substrate by a simple microwave hydrothermal reaction in an aqueous solution containing sodium tellurite and hydrazine monohydrate. Experimental details are described in the Supporting Information.

The X-ray diffraction (XRD) pattern of the Zn/ZnO structure (ZA) showed both Zn and ZnO peaks (Figure 1 a). The ZnO peaks could be indexed as a hexagonal wurtzite ZnO structure with calculated lattice constants of $a = 0.3242$ nm and $c = 0.5201$ nm. A relatively high intensity ZnO (002) peak indicated a high degree of alignment of the ZnO nanowires. The XRD peak intensity of the Zn/ZnO/ZnTe structure (ZT) was much lower. The (111), (220), and other peaks were identified for the zinc-blende ZnTe structure with a lattice constant of $a = 0.6039$ nm. The UV/Vis absorption spectra of the ZA and ZT nanostructure arrays are shown in Figure 1 b. ZA showed a strong absorption in the UV region characteristic of the wide-band-gap ZnO. However, the absorption of ZT was dramatically shifted into the visible region. These vastly different absorption spectra are reflected in the vivid reddish color of ZT in contrast to white ZA, as shown in Figure 1 b; thus, ZT is expected to absorb a much wider range of the solar spectrum than ZA, which absorbs only UV light.

[*] Dr. J.-W. Jang,[+] Dr. G. Magesh,[+] Dr. J. Y. Kim, Prof. J. K. Seo, Prof. J. S. Lee
School of Energy and Chemical Engineering
Ulsan National Institute of Science and Technology (UNIST)
50 UNIST-gil, Ulsan, 689-798 (South Korea)
E-mail: jlee1234@unist.ac.kr
Dr. S. Cho,[+] Y. J. Jang, W. Y. Kim, Prof. S. Kim, Prof. K.-H. Lee
Department of Chemistry/Chemical Engineering
Pohang University of Science and Technology (POSTECH)
San 31, Hyoja-Dong, Pohang, 790-784 (South Korea)
E-mail: ce20047@postech.ac.kr
[+] These authors contributed equally.

[**] This research was supported by grants from the BK + Program, the Basic Science Research Program (No. 2012-017247), and the Korea Center for Artificial Photosynthesis (KCAP) funded by the National Research Foundation of Korea (No. 2012M1A2A2671779).

Supporting information for this article, including details of the synthesis of ZnO nanowire arrays, the synthesis of the ZnO/ZnTe structure, and the photoelectrochemical reduction of CO_2, analysis of the products of CO_2 reduction, and characterization of the materials investigated, is available on the WWW under http://dx.doi.org/10.1002/anie.201310461.

 © 2014 Wiley-VCH Verlag GmbH & Co. KGaA, Weinheim

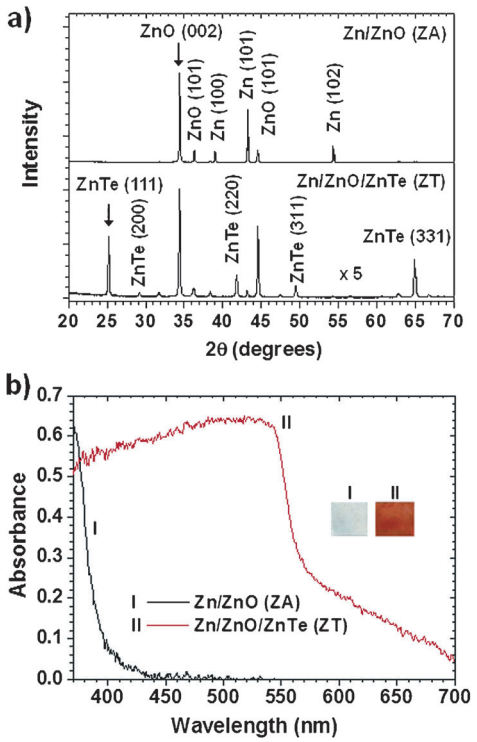

Figure 1. a) XRD patterns of the Zn/ZnO structure (ZA) and the Zn/ZnO/ZnTe structure (ZT). b) UV/Vis absorption spectra of ZA and ZT. The inset shows photographs of ZA and ZT under room light.

Figure 2 a,b shows SEM images of ZnO nanowires that are aligned on the Zn substrate (ZA). The average diameter of these nanowires with smooth surfaces was approximately 70 nm (Figure 2 b). After the microwave hydrothermal reaction, ZnTe blocks comprised of cubic-shaped grains capped the upper part of the ZnO nanowires (Figure 2 c,d). Figure 2 e displays the TEM image of a ZnTe block, and its selected-area electron diffraction (SAED) pattern in Figure 2 f shows hexagonally arranged spots, which indicate the single-crystalline nature of the ZnTe grains. Figure 2 g shows a high-resolution (HR) TEM image of the ZnTe grain marked by the circle in Figure 2 e. The lattice spacing of 0.305 nm corresponds to the distance between the (200) lattice planes of zinc-blende ZnTe crystals.[9] A schematic illustration of the structure of ZT formed on the ZnO nanowire array is shown in Figure 2 h. As mentioned, this crystal-growth process represents the simplest way to synthesize ZnTe in an aqueous solution without using a surfactant.

The mechanism of the ZnO-to-ZnTe conversion appears similar to the dissolution–recrystallization mechanism observed for ZnO-to-ZnSe conversion.[22,23] The source of Zn for the formation of crystalline ZnTe is the ZnO nanowires themselves. Under alkaline conditions in the presence of hydrazine, hydroxide ions react with ZnO surfaces, and $Zn(OH)_4^{2-}$ is released.[10,22,23] Tellurite (TeO_3^{2-}) ions in the reaction solution are reduced first by hydrazine to tellurium (Te) atoms or clusters as the reaction temperature increases, and undergo further reduction or disproportionation in the alkaline solution to generate Te^{2-} ions.[11,24] However, at a low concentration (0.075 M) of hydrazine, only Te metal was produced, although ZnSe was formed at the same concentration in the ZnO-to-ZnSe conversion.[22] For the conversion of ZnO into ZnTe, a hydrazine concentration of at least 0.3 M is essential. This difference could arise from the more negative standard electrode potential of Te ($E^o = -1.14$ V) than that of selenium ($E^o = -0.91$ V).[25] After dissolution of the Te^{2-} ions, Te^{2-} ions and $Zn(OH)_4^{2-}$ underwent recrystallization to form ZnTe crystallites by heterogeneous nucleation and growth on the ZnO nanowires.[10,11]

To investigate the band positions of the synthesized ZT nanostructures, we conducted Mott–Shottky and Tauc analyses (see Figure S1 in the Supporting Information). The flat-band potentials of the ZT electrodes were determined by taking the x intercept of a linear fit to the Mott–Schottky plot as a function of applied potential.[26,27] The sign of the slope of this plot indicates that the ZT electrode is a p-type electrode. The flat-band potential and thereby the valence-band position determined from this plot was 0.68 V (vs. RHE).[28] The charge-carrier density obtained from the slope of the Mott–

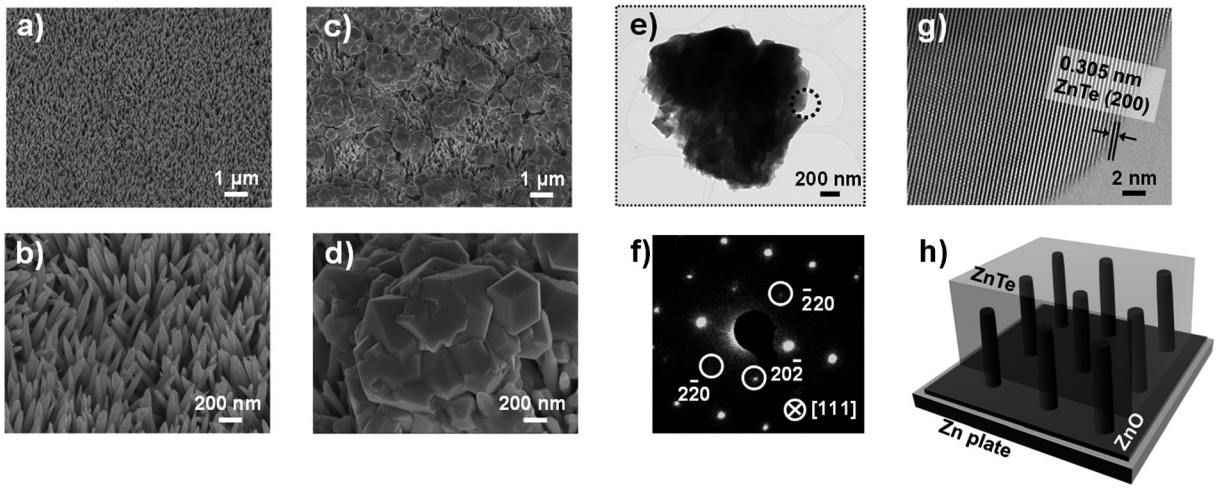

Figure 2. a–d) Tilted SEM images of the Zn/ZnO structure (ZA; a, b) and the Zn/ZnO/ZnTe structure (ZT; c, d); e) TEM image of a ZnTe block; f) SAED pattern of the structure; g) HR TEM image of the area indicated by the circle in (e); h) schematic illustration of the ZT structure.

 © 2014 Wiley-VCH Verlag GmbH & Co. KGaA, Weinheim

Schottky plots was 5.09×10^{17} cm^{-3}. The optical band-gap energy of ZT was estimated to be approximately 2.15 eV from the absorption spectra by using the Tauc plot, in agreement with the previously reported values (2.1 and 2.26 eV).[1,10] From the results, the conduction-band-edge position was calculated as −1.48 V versus RHE. This experimental value is a little less negative than the reported value for ZnTe (−1.63 V).[6,7] The obtained flat-band potential could have been affected by many factors, including the surface composition, the termination and concentration of trap states, and coupling with ZnO.[29,30]

The conduction-band-edge positions of different p-type semiconductors and the standard reduction potentials for CO_2-reduction reactions are summarized in Figure 3.[8,31–33] In

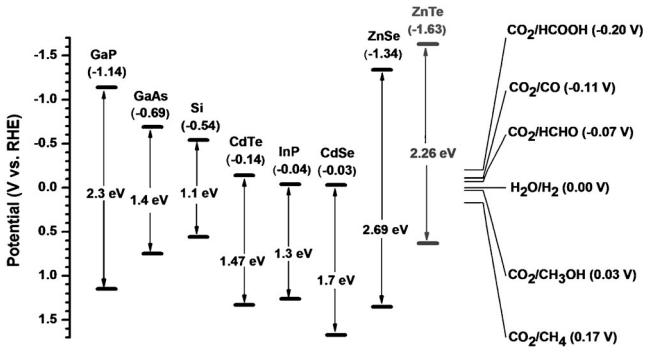

Figure 3. The conduction-band energy levels (in parenthesis) of various p-type semiconductors and ZnTe in relation to the standard reduction potentials of different CO_2-reduction reactions.[8,22–25]

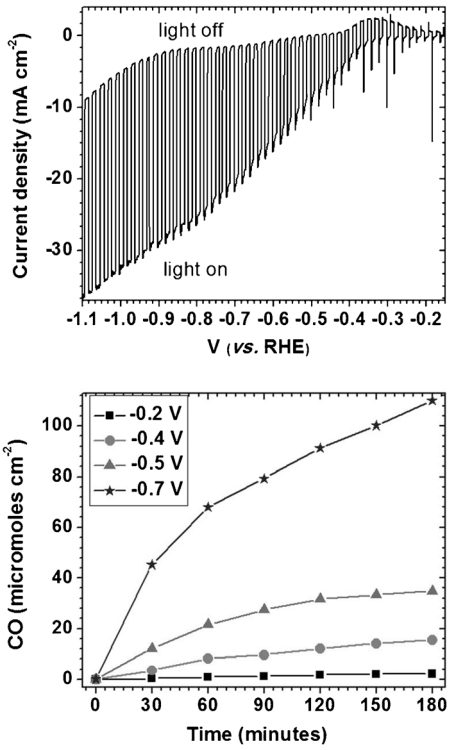

Figure 4. a) Photocurrent–potential characteristics of the H_2 evolution and CO_2 reduction with the Zn/ZnO/ZnTe (ZT) cathode, a Pt anode, and a Ag/AgCl reference electrode in 0.5 M aqueous $KHCO_3$ (pH 7.5) under irradiation with a 500 W Hg lamp (> 420 nm cutoff filter, 490 mW cm^{-2}) at a scan rate of 5 mV s^{-1}. b) Quantity of CO formed as a function of the reaction time at different potentials (vs. RHE).

comparison to other p-type semiconductors reported for CO_2 reduction, the conduction-band edge of ZnTe is located at the most negative energy, at −1.63 V (−1.48 V, experimental), followed by those of ZnSe and GaP at −1.34 and −1.14 V, respectively.[8,31] Thus, electrons in the conduction band of ZnTe have a higher driving force to carry out the reduction reaction than the other semiconductor photocatalysts.[7]

The ZT photocathode was applied to CO_2 reduction to gauge its potential in PEC artificial photosynthesis. Since the reduction potentials for the reduction of CO_2 to HCOOH, CO, and HCHO are more negative than that for water reduction, the most negative conduction-band edge of ZnTe makes its application for CO_2 reduction particularly interesting. Figure 4 a shows the current–potential curve for the CO_2 reduction in 0.5 M aqueous $KHCO_3$ (pH 7.5) under irradiation with a 500 W Hg lamp (with > 420 nm cutoff filter, 490 mW cm^{-2}). The photocurrent density of the ZT photocathode approaches 30 and 20 mA cm^{-2} at −0.9 and −0.7 V versus RHE, respectively. When a solar simulator (100 mW cm^{-2}) was used, it showed 11.8 and 8.2 mA cm^{-2} at −0.9 and −0.7 V versus RHE, respectively (see Figure S2), which are more than one third of the values obtained with the 500 W Hg lamp with a cutoff filter (490 mW cm^{-2}). The reasons why the photocurrents do not show a proportional increase with the increased light intensity could be decreased absorption efficiency under the high photon flux and the limited absorption spectrum because of the cutoff filter (> 420 nm).

Recently reported ZnO/ZnTe core–shell nanowires synthesized by chemical vapor deposition (CVD) showed an anodic current of only few nA and did not show a cathodic current.[34] Even though our synthetic process is based on a simple solution-phase method, ZnTe synthesized in this study possessed a very high crystallinity and formed a intimate heterojunction with ZnO nanowires. These factors may be responsible for the high photocurrent densities of our ZT photocathode.

The ZT electrode showed the best performance when the growth time of ZnO and ZnTe was 1.5 and 2 h, respectively. When the ZnO nanowire growth time was too short, the photocurrent was low owing to the limited Zn supply for ZnTe formation. When the ZnO nanowire growth time was too long, the photocurrent also decreased owing to the increased length of the ZnO nanowires. The ZnO nanowires act as a charge-transfer medium between ZnTe and Zn plate, and thus excessively long ZnO wires increase the chance of charge recombination. Likewise, a short ZnTe growth time results in insufficient ZnTe formation, and excessive ZnTe formation with too long a growth time leads to a deterioration in electrolyte permeation. The optimized system showed a significant reduction current from −1.1 to −0.2 V versus RHE. Above −0.2 V, a negligible reduction current was observed. The ZA electrode did not show any photoresponse under the negative potential because ZnO is an n-type semiconductor.

 © 2014 Wiley-VCH Verlag GmbH & Co. KGaA, Weinheim

The CO_2-reduction experiments were carried out between −0.7 and −0.2 V (Figure 4b). Corresponding chronoamperometry data are shown in Figure S3 of the Supporting Information. The reduction of CO_2 resulted in the formation of CO, whose quantity at different potentials in the $KHCO_3$ medium is shown in Figure 4b; the faradaic efficiencies are given in Table 1 (see also Table S1 in the Supporting Information). The amount of CO formed increased with an increase in potential and time. The faradaic efficiency for CO remained at around 9% at −0.2 and −0.4 V, then increased with an increase in bias potential to reach 22.9% at −0.7 V after 1 h. Besides CO, hydrogen was also obtained during the reaction, the formation of which accounted for 50–60% of the corresponding currents (Table 1; see also Figure S4). The faradaic efficiency for the formation of CO decreased but there was no significant change in the amount of H_2 formation as the ZnTe underwent photocorrosion during the reaction (see Table S1 and Figure S4 in the Supporting Information and Figure 4b).This result indicates that CO_2 reduction is more sensitive to the state of ZnTe than hydrogen evolution.

Table 1: Products of the photoelectrochemical reduction of CO_2 in 0.5 M aqueous $KHCO_3$.[a]

Potential (V vs. RHE)	Charge [C]	Faradaic efficiency [%] CO	H_2
−0.2	2.2	8.4	56.6
−0.4	14.8	10.7	60.4
−0.5	20.6	18.2	44.3
−0.7	58.4	22.9	60.7

[a] Products obtained with the Zn/ZnO/ZnTe photocathode and a Pt anode after irradiation with a 500 W Hg lamp (>420 nm cutoff filter, 490 mW cm^{-2}) for 1 h.

When the electrolyte was changed to $NaHCO_3$, the selectivity of the reduction of CO_2 on the ZT electrode was dramatically reduced to 11.0, whereas in aqueous tetrabutylammonium bromide (TBABr), the selectivity for CO as the reduction product increased to 34.9%, thus showing a noticeable cation effect[35] (see Figure S5 and Table S2). The size of K^+ is larger than that of Na^+ but smaller than that of TBA^+. The larger TBA^+ ion is less solvated by water and is thus better adsorbed than the smaller Na^+ ion to the electrode surface. It can therefore stabilize the $CO_2^{\bullet-}$ ion species (intermediate in the formation of CO) and deter adsorption of the H^+ ion (intermediate in the formation of H_2).[35] However, in both cases, the stability and performance of the ZT electrode were lower than in $KHCO_3$. These results illustrate the importance of the appropriate electrolyte for CO_2 reduction.

In all experiments described above, the total faradaic efficiency for the formation of the gas product was not 100%. Thus, we tried to identify the liquid products by various analytical techniques, such as HPLC, NMR spectroscopy, and mass spectrometry. However, we could not find any liquid product, thus implying that the rest of the photocurrent must be balanced, mostly by photocorrosion under the applied bias. Even though there was considerable photocorrosion, our ZT electrode always showed a relatively stable photocurrent and relatively stable product formation as compared with other bare ZnTe electrodes, which usually lose their performance in a few seconds, especially at an applied potential below −0.4 V versus RHE.[36]

X-ray photoelectron spectroscopy (XPS) of the ZT electrode showed the Te^{4+} $3d_{5/2}$ peak at 577.2 eV and Te^{4+} $3d_{3/2}$ at 587.5 eV. These peaks correspond to TeO_2 binding energies (see Figure S6)[37] and are even higher than those of ZnTe (Te^{2-} $3d_{5/2}$ peak at 573.4 eV and Te^{2-} $3d_{3/2}$ at 583.9 eV). The atomic ratio of Zn/Te is also lower than 1 (0.73; see Table S3), thus indicating that there exist TeO_x phases on the surface of crystalline ZnTe phases that seem to be formed during the cooling process after ZnTe formation. The TeO_x species is amorphous with no distinct XRD pattern. The shoulder absorption beyond about 580 nm in the UV/Vis spectrum (Figure 1b) also seems to be due to absorption by amorphous TeO_x.[38] Under a high applied potential (−0.7 V vs. RHE), the Te^{2-} $3d_{5/2}$/Te^{4+} $3d_{5/2}$ peak ratio decreased from 0.54 to 0.41, and the Zn/Te atomic ratio increased from 0.73 to 1.19 through the photocorrosion of ZnTe to Zn and the Te^{2-} ion. Under a low applied potential (−0.2 V vs. RHE), the Te^{2-} $3d_{5/2}$/Te^{4+} $3d_{5/2}$ ratio decreased to 0.46, and the Zn/Te atomic ratio also decreased to 0.65 through the photocorrosion of ZnTe now to Te and the Zn^{2+} ion (see Table S3).[36] Both reactions occur under dark conditions and are the reason for the negative and positive dark currents at low and high applied bias, respectively (Figure 4a).

The lowest potentials reported so far for the reduction of CO_2 with p-type semiconductors and ZT are compared in Table S4 of the Supporting Information. There are many other unlisted examples of CO_2 reduction with p-type semiconductors, but they need much higher overpotentials than those in Table S4. Among the bare photocatalysts without a noble-metal cocatalyst, the ZT photocathode shows the lowest potential for the reduction of CO_2 to CO, although this potential is still higher than that of a cocatalyst-loaded semiconductor (Au/p-Si, −0.09 V) or a hybrid semiconductor (CuO–Cu_2O, +0.07).[39–41] For example, bare p-type silicon (p-Si) was reported to require −0.62 or −0.54 V to carry out the reaction, whereas p-GaP required −0.61 V.[39,40,42] The only bare photocatalysts which required comparable potentials to that of ZnTe were p-CdTe and p-InP with around −0.35 V.[43]

To demonstrate that the formation of CO results only from the reduction of CO_2, we carried out a control reaction under similar conditions by replacing CO_2 with N_2. To rule out the electrochemical reduction of CO_2, we also carried out an experiment in the dark under similar conditions. Both reactions did not result in the formation of CO, thus confirming that CO is formed exclusively by the photoelectrochemical reduction of CO_2.

We measured the incident-photon-to-current-conversion efficiency (IPCE) to study the photoresponse of the photocathode as a function of the wavelength of incident light (Figure 5). The IPCE is defined by the following equation:

$$\mathrm{IPCE} = [J\,1240]/[P_{mono}\,\lambda] \quad (1)$$

 © 2014 Wiley-VCH Verlag GmbH & Co. KGaA, Weinheim

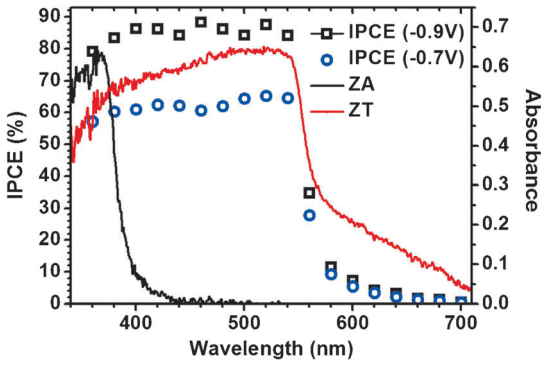

Figure 5. Incident-photon-to-current-conversion efficiency (IPCE) of ZT at −0.9 and −0.7 V versus RHE and UV/Vis spectra of ZT and ZA.

in which J is the photocurrent density (mA cm^{-2}), P_{mono} is the light power density (mW cm^{-2}) at λ, and λ is the wavelength of incident light (nm). The IPCE behavior followed the UV/Vis absorption spectrum fairly well, thus demonstrating that the majority of the absorbed light of different wavelengths contributed to photocurrent generation by H_2 evolution and CO_2 reduction. The ZT photocathode exhibited over 60 and 85% IPCE in the range of 400–550 nm at −0.7 and −0.9 V versus RHE, respectively, thus indicating that ZnTe could be a highly efficient photocathode.

In summary, the ZnTe/ZnO/Zn electrode was directly fabricated through the reaction of ZnO nanowire arrays on a Zn metal substrate with an aqueous solution of tellurite and hydrazine. The ZT photocathode was applied to photoelectrochemical CO_2 reduction. The formation of CO and hydrogen was observed at −0.7–−0.2 V versus RHE in aqueous $KHCO_3$ with high IPCE values (ca. 60% and ca. 85% at −0.7 and −0.8 V vs. RHE, respectively). The ZT photocathode also showed a stable photocurrent and CO formation even at −0.2 V versus RHE. These results demonstrate that ZnTe has high prospects to be an efficient CO_2-reduction photocatalyst. There is ample room for improvement, particularly in the selectivity for CO_2 reduction (instead of water reduction) and stability against corrosion. The combination of ZnTe with suitable molecular and/or inorganic cocatalysts could alleviate both of these problems,[8,19,21] and research in this direction is under way.

Received: December 3, 2013
Published online: April 16, 2014

Keywords: artificial photosynthesis · photocathodes · photoelectrochemical CO_2 reduction · solution synthesis · zinc telluride

[1] T. Mahalingam, V. S. John, S. Rajendran, P. J. Sebastian, *Semicond. Sci. Technol.* **2002**, *17*, 465–470.
[2] L. Li, Y. Yang, X. Huang, G. Li, L. Zhang, *J. Phys. Chem. B* **2005**, *109*, 12394–12398.
[3] T. Tanaka, K. Saito, M. Nishio, Q. Guo, H. Ogawa, *Appl. Phys. Express* **2009**, *2*, 122101.
[4] Q. Wu, M. Litz, X. C. Zhang, *Appl. Phys. Lett.* **1996**, *68*, 2924.
[5] J. Schrier, D. O. Demchenko, L.-W. Wang, *Nano Lett.* **2007**, *7*, 2377–2382.
[6] S. Kaniyankandy, S. Rawalekar, S. Verma, H. N. Ghosh, *J. Phys. Chem. C* **2011**, *115*, 1428–1435.
[7] J. Zhang, S. Jin, H. C. Fry, S. Peng, E. Shevchenko, G. P. Wiederrecht, T. Rajh, *J. Am. Chem. Soc.* **2011**, *133*, 15324–15327.
[8] B. Kumar, M. Llorente, J. Froehlich, T. Dang, A. Sathrumm, C. P. Kubiak, *Annu. Rev. Phys. Chem.* **2012**, *63*, 541–569.
[9] S. H. Lee, Y. J. Kim, J. Park, *Chem. Mater.* **2007**, *19*, 4670–4675.
[10] S. Xu, C. Wang, Q. Xu, H. Zhang, R. Li, H. Shao, W. Lei, Y. Cui, *Chem. Mater.* **2010**, *22*, 5838–5844.
[11] Y. Li, Y. Ding, Z. Wang, *Adv. Mater.* **1999**, *11*, 847–850.
[12] K. Yong, Y. Sahoo, H. Zeng, M. T. Swihart, J. R. Minter, P. N. Prasad, *Chem. Mater.* **2007**, *19*, 4108–4110.
[13] A. Fiore, R. Mastria, M. G. Lupo, G. Lanzani, C. Giannini, E. Carlino, G. Morello, M. De Giorgi, Y. Li, R. Cingolani, L. Manna, *J. Am. Chem. Soc.* **2009**, *131*, 2274–2282.
[14] J. Zhang, K. Sun, A. Kumbhar, J. Fang, *J. Phys. Chem. C* **2008**, *112*, 5454–5458.
[15] M. Grätzel, *Nature* **2001**, *414*, 338–344.
[16] J. A. Turner, *Science* **2004**, *305*, 972–974.
[17] M. Halmann, *Nature* **1978**, *275*, 115–116.
[18] G. Magesh, E. S. Kim, H. J. Kang, M. Banu, J. Y. Kim, J. H. Kim, J. S. Lee, *J. Mater. Chem. A* **2014**, *2*, 2044–2049.
[19] K. S. Joya, Y. F. Joya, K. Ocakoglu, R. van de Krol, *Angew. Chem.* **2013**, *125*, 10618–10630; *Angew. Chem. Int. Ed.* **2013**, *52*, 10426–10437.
[20] F. F. Abdi, L. Han, A. H. M. Smets, M. Zeman, B. Dam, R. van de Krol, *Nat. Commun.* **2013**, *4*, 2195.
[21] K. S. Joya, N. K. Subbaiyan, F. D'Souza, H. J. M. de Groot, *Angew. Chem.* **2012**, *124*, 9739–9743; *Angew. Chem. Int. Ed.* **2012**, *51*, 9601–9605.
[22] S. Cho, J.-W. Jang, S. H. Lim, H. J. Kang, S.-W. Rhee, J. S. Lee, K. H. Lee, *J. Mater. Chem.* **2011**, *21*, 17816–17822.
[23] S. Cho, J.-W. Jang, J. Kim, J. S. Lee, W. Choi, K.-H. Lee, *Langmuir* **2011**, *27*, 10243–10250.
[24] A. U. Ubale, R. J. Dhokne, P. S. Chikhikar, V. S. Sangawar, D. K. Kulkarni, *Bull. Mater. Sci.* **2012**, *29*, 165–168.
[25] P. C. Hayes, S. H. Algie, *Process Principles in Minerals and Materials Production*, Hayes, **1993**, pp. 660–665.
[26] F. Cardon, W. P. Gomes, *J. Phys. D* **1978**, *11*, L63.
[27] S. Cho, J. W. Jang, K. J. Kong, E. S. Kim, K. H. Lee, J. S. Lee, *Adv. Funct. Mater.* **2013**, *23*, 2348–2356.
[28] T. Jiang, T. Xie, L. Chen, Z. Fu, D. Wang, *Nanoscale* **2013**, *5*, 2938–2944.
[29] H. Ge, H. Tian, Y. Zhou, S. Wu, D. Liu, X. Fu, X.-M. Song, X. Shi, X. Wang, N. Li, *ACS Appl. Mater. Interfaces* **2014**, *6*, 2401–2406.
[30] C. Du, X. Yang, M. T. Mayer, H. Hoyt, J. Xie, G. McMahon, G. Bischoping, D. Wang, *Angew. Chem.* **2013**, *125*, 12924–12927; *Angew. Chem. Int. Ed.* **2013**, *52*, 12692–12695.
[31] E. E. Benson, C. B. Kubiak, A. J. Santhrum, J. M. Smieja, *Chem. Soc. Rev.* **2009**, *38*, 89–99.
[32] A. Paracchino, V. Laporte, K. Sivula, M. Grätzel, E. Thimsen, *Nat. Mater.* **2011**, *10*, 456–461.
[33] C.-Y. Chiang, Y. Shin, K. Aroh, S. Ehrman, *Int. J. Hydrogen Energy* **2012**, *37*, 8232–8239.
[34] Y. Lin, W.-J. Chen, J. Y. Lu, Y. H. Chang, C.-T. Liang, Y. F. Chen, J.-Y. Lu, *Nanoscale Res. Lett.* **2012**, *7*, 401.
[35] M. R. Thorson, K. I. Siil, P. J. A. Kenis, *J. Electrochem. Soc.* **2013**, *160*, 69–74.
[36] J. O'M. Bockris, K. Uosaki, *J. Electrochem. Soc.* **1977**, *124*, 1348–1355; K. Uosaki, "The Photoelectrochemical Production of Hydrogen" can be found under http://hdl.handle.net/2115/42803, **1976**, pp. 127–135.

 © 2014 Wiley-VCH Verlag GmbH & Co. KGaA, Weinheim

[37] M. A. Ford, M. Want, A. P. Smart, C. M. S. Torres, C. D. W. Wiikinsont, W. Kuhns, H. P. Wagner, S. Bauers, H. Leiderers, W. Gebhardts, *Semicond. Sci. Technol.* **1991**, *6*, 115 – 122.
[38] R. Nayak, V. Gupta, A. L. Dawar, K. Sreenivas, *Thin Solid Films* **2003**, *445*, 118 – 126.
[39] R. Hinogami, Y. Nakamura, S. Yae, Y. Nakato, *J. Phys. Chem. B* **1998**, *102*, 974 – 980.
[40] L. Junfu, C. Baozhu, *J. Electroanal. Chem.* **1992**, *324*, 191 – 200.
[41] G. Ghadimkhani, N. R. de Tacconi, W. Chanmanee, C. Janaky, K. Rajeshwar, *Chem. Commun.* **2013**, *49*, 1297 – 1299.
[42] H. Noda, A. Yamamoto, S. Ikeda, M. Maeda, K. Ito, *Chem. Lett.* **1990**, *19*, 1757 – 1760.
[43] H. Yoneyama, K. Sugimura, S. Kuwabata, *J. Electroanal. Chem.* **1988**, *249*, 143 – 153.

 © 2014 Wiley-VCH Verlag GmbH & Co. KGaA, Weinheim